OPTIMIZATION OF MAGNETIC FIELD PARAMETERS IN AMD FOR ENHANCED POSITRON YIELD*

Xin Xu[1], Tian Xia[1], Zihao Wang[1], Hanzhe Niu[1], Guoxi Pei[1], Qing Luo[†1], Ailin Zhang[‡1]
[1]University of Science and Technology of China, hefei, China

Abstract

To address the demand for high positron capture efficiency in high-luminosity electron-positron colliders, this paper systematically investigates the influence of magnetic field distributions within the Adiabatic Matching Device (AMD) on positron yield. Parametric studies of the conventional Flux Concentrator (FC) reveal that the intrinsic initial field ramp-up region creates a critical physical bottleneck, necessitating a trade-off between suppressing non-adiabatic radial kicks and mitigating transverse envelope expansion. To circumvent these constraints, optimization laws are derived using an idealized model, demonstrating that maximizing effective capture dictates the integration of intense peak fields with compact decay lengths to synergistically manage transverse transmission and longitudinal phase slippage. Furthermore, three candidate superconducting (SC) schemes for the Super Tau-Charm Facility (STCF) are evaluated under normalized drift distances to isolate magnetic effects. Simulation results confirm that the 18 T low-temperature superconducting (LTS) solenoid achieves the highest positron yield, benefiting from superior peak field intensity and enhanced transverse confinement. This work provides a physical rationale for the development of next-generation high-field AMD for high-intensity positron sources.

INTRODUCTION

As luminosities of next-generation colliders (e.g., FCC-ee, CEPC, STCF) escalate, positron sources demand unprecedented capture efficiencies. An Adiabatic Matching Device (AMD), typically a Flux Concentrator (FC) [1–4], is essential for phase-space matching downstream of the target. However, conventional FCs face severe physical and engineering constraints: geometric and insulation requirements create an unavoidable initial field ramp-up region that degrades matching, while extreme pulsed currents pose severe breakdown risks, effectively capping peak fields [5].

To circumvent these bottlenecks, superconducting (SC) solenoids offer a promising alternative [6]. They provide steady-state, ultra-high peak fields (e.g., > 15 T) and eliminate the initial ramp-up region by immersing the target at the field peak. In this work, the initial positron distributions are generated via Geant4 target simulations [7], yielding a total initial positron coefficient of 7.01 e^+/e^- at the target exit. Subsequent beam dynamics tracking throughout the AMD is performed using ASTRA [8]. It should be noted that all simulations in this study are consistently terminated at the entrance of the first downstream accelerating structure. Utilizing these tools, this paper systematically investigates AMD yield optimization: we first analyze yield sensitivity to FC ramp-up parameters, then employ an idealized model to identify the dynamical laws governing peak field and decay length, and finally evaluate three realistic SC schemes for the STCF to establish a physical rationale for next-generation AMD selection.

ANALYZING YIELD VIA FC PARAMETER SWEEPS

Influence of B_0 and ΔZ on Positron Yield

In practical engineering applications of FC, the conversion target is typically situated within the magnetic field ramp-up region due to geometric constraints of the target assembly and radiation shielding requirements. The magnetic field distribution in this region, as illustrated in Fig. 1, is characterized by the initial field at the target exit (B_0), the ramp length to the peak field (ΔZ), and the subsequent adiabatic decay length (L).The yield calculation is restricted to the 0 MeV to 20 MeV range, as positrons in this lower energy regime constitute the vast majority of the initial yield emerging from the target [9, 10].

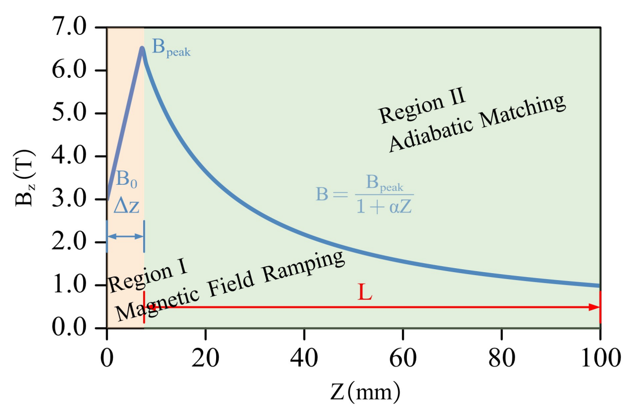

Figure 1: Typical magnetic field profile generated by an FC.

To systematically evaluate the impact of this initial ramp-up region on capture efficiency, the peak field B_{peak} was initially fixed at 6.0 T. This value aligns with the typical 4 T to 7 T peak fields achieved in conventional normal-conducting pulsed FC designs [4, 5], representing a technologically mature and safe engineering baseline. The physical aperture features an entrance radius of 3.5 mm and an exit radius of 26 mm. As shown in Fig. 2, increasing B_0 significantly enhances the positron yield, which is attributed to the higher initial field providing a stronger focusing force that effectively suppresses the rapid expansion of positrons with large

* Work supported by STCF
† luoqing@ustc.edu.cn
‡ ailinz@ustc.edu.cn

divergence angles. The influence of ΔZ on yield is non-monotonic and depends heavily on the value of B_0. At lower initial fields ($B_0 \leq 4.0$ T), the yield decreases monotonically as ΔZ increases. In this regime, the initial field is insufficient to confine high-divergence particles; increasing ΔZ forces particles to traverse a longer drift distance in a weak field, leading to continuous envelope expansion and severe transverse losses due to physical aperture collisions.

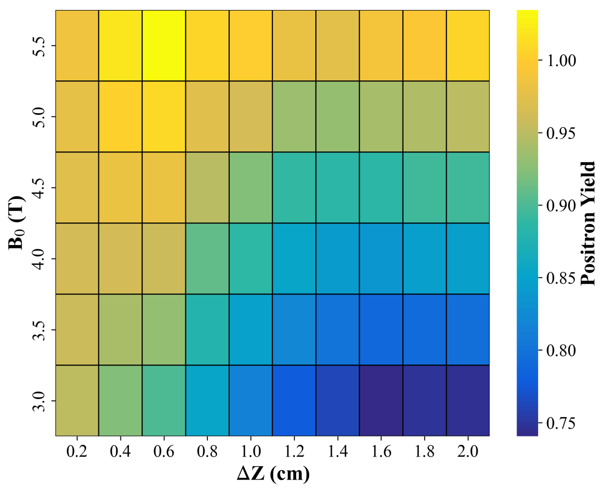

Figure 2: Positron yield as a function of the initial field B_0 and the ramp length ΔZ.

Conversely, when $B_0 \geq 4.5$ T, the initial transverse divergence is partially controlled, and the yield response to ΔZ shifts to a non-monotonic evolution, peaking around $\Delta Z \approx 0.6$ cm. If ΔZ is too short, the extreme axial field gradient $\partial B_z / \partial z$ introduces a substantial radial field component, which exerts a violent transverse kick on high-energy particles, inducing abrupt envelope perturbations and subsequent losses. However, an excessively long ΔZ causes the particles to undergo excessive envelope expansion before reaching the peak field, again triggering transverse losses. These results indicate that parameter selection for the FC ramp-up region essentially involves seeking an optimal balance in transverse dynamics between suppressing non-adiabatic kicks and limiting excessive envelope expansion.

Influence of L and B_{peak} on Positron Yield

Following the optimization of the initial field ($B_0 = 5.5$ T) and ramp length ($\Delta Z = 0.6$ cm), the influence of the decay length L and peak field B_{peak} on positron yield was further evaluated. As illustrated in Fig. 3(a), the yield follows a non-monotonic trend with L, reaching a maximum at approximately 18 cm, whereas the bunch length increases monotonically across the scanned range. Furthermore, two B_0 scaling strategies were compared during the B_{peak} parameter sweep: (1) a fixed-ratio strategy, maintaining a constant B_{peak}/B_0 to preserve the normalized axial field profile; and (2) a fixed-difference strategy, maintaining a constant $B_{\text{peak}} - B_0$ to ensure a stable absolute axial gradient $\partial B_z / \partial z$.

Simulation results (Fig. 3(b)) reveal that while the positron yield grows significantly during the initial stages of field en-

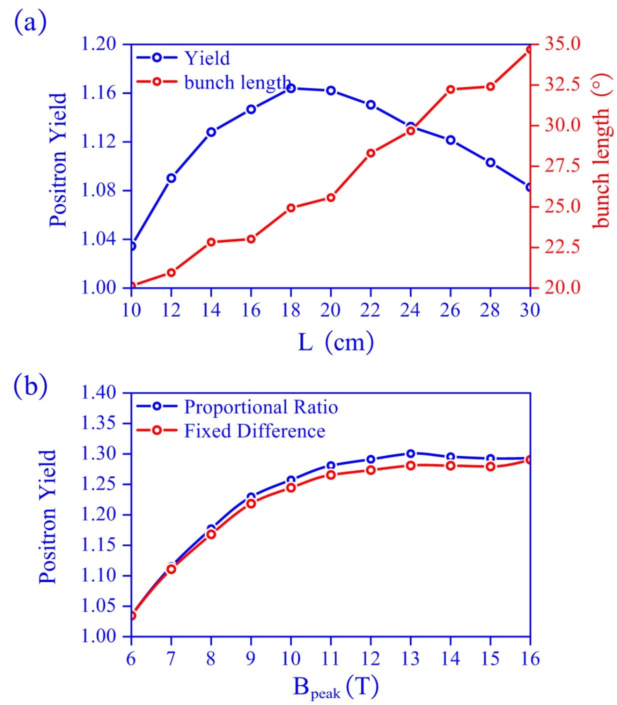

Figure 3: Positron yield as a function of (a) the decay length L, and (b) the peak field B_{peak}.

hancement, it encounters a clear saturation plateau once B_{peak} exceeds 12.0 T, regardless of the scaling strategy. This underscores the marginal diminishing returns of simply increasing the peak field within the structural constraints of conventional pulsed FC.

Systematic scans reveal multiple dynamical constraints facing traditional FC: the initial ramp-up region limits transverse capture, the decay region must balance transverse and longitudinal matching, and the yield gain saturates heavily beyond 12 T. These findings demonstrate that the inherent structural configuration of the FC has become a physical bottleneck for further yield enhancement.Consequently, to overcome these fundamental bottlenecks, transitioning to superconducting (SC) schemes represents a compelling avenue for next-generation designs.

OPTIMIZING YIELD WITHIN IDEALIZED FIELDS

Unlike the traditional Flux Concentrator (FC) whose tight geometric constraints inherently introduce a detrimental field ramp-up region, next-generation superconducting (SC) AMD architectures offer the engineering feasibility to directly immerse the conversion target at the field peak while accommodating a much larger physical aperture. Inspired by this structural advantage, an idealized adiabatic model ($B_{\text{peak}} = B_0, \Delta Z = 0$) was established to explore the theoretical performance limits of such configurations. The longitudinal magnetic field distribution of this model is analytically described by the classic AMD profile:

$$B(z) = \frac{B_{\text{peak}}}{1 + \alpha z} \quad (1)$$

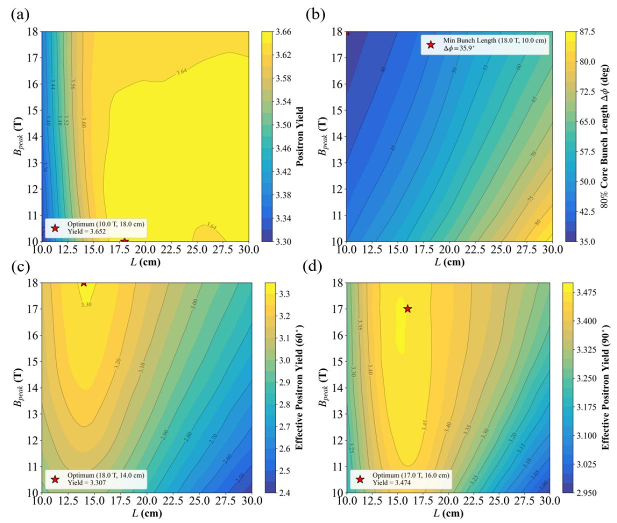

Figure 4: Influence of B_{peak} and L on (a) positron yield, (b) core bunch length (80 % particles), (c) positron yield within 60° microwave phase, and (d) positron yield within 90° microwave phase under ideal AMD conditions.

where α is the field decay coefficient, which determines the decay length L. It should be noted that while practical coil configurations and fringe field effects may prevent a perfect replication of this theoretical profile, this analytical model serves as an essential physics benchmark. To investigate the coupled impacts of B_{peak} and L under these ideal conditions, a constant physical aperture with a diameter of 60 mm is applied throughout this model.

As shown in Fig. 4(a), the total yield saturates at $L > 16.0$ cm and $B_{\text{peak}} > 10.0$ T. However, when introducing representative phase cutoffs within the downstream normal-conducting structures operating at an S-band frequency of 2856 MHz, the peak effective yield consistently shifts toward the region of higher field intensities and compact decay lengths, as illustrated in Fig. 4(c) and (d). Specifically, a high B_{peak} (e.g., 18 T) effectively suppresses longitudinal bunch expansion (Fig. 4(b)) by accelerating the transverse-to-longitudinal momentum transfer. It should be clarified that in this idealized parameter scan, the entrance of the downstream accelerating structure is fixed at 10 cm downstream of the AMD exit, with a 0.5 T DC magnetic field employed to bridge this intermediate drift section. Although this simplified spatial distribution may not represent a fully optimized engineering layout and requires further practical optimization in future studies, the current evaluation adequately demonstrates that high-field AMD configurations with shorter structural lengths are structurally advantageous for maximizing the capturable positron yield.

EVALUATING YIELD IN REALISTIC DESIGNS

This section evaluates three candidate superconducting AMD schemes for the STCF: 15 T HTS, 15 T LTS, and 18 T LTS (profiles in Fig. 5). To ensure a consistent comparison and isolate magnetic effects from natural velocity dispersion, the total drift distance to the downstream structure entrance was fixed for all schemes, with a 0.5 T DC solenoid field used to bridge any remaining gaps. These realistic longitudinal magnetic field profiles were numerically obtained via 3D finite-element simulations using the OPERA. It is worth noting that under the same peak field of 15 T, the HTS configuration exhibits a significantly sharper field decay compared to its LTS counterpart. This discrepancy is fundamentally dictated by the higher critical current density of high-temperature superconductors, which allows for a much more compact coil geometry that concentrates the magnetic flux and accelerates the axial field drop-off.

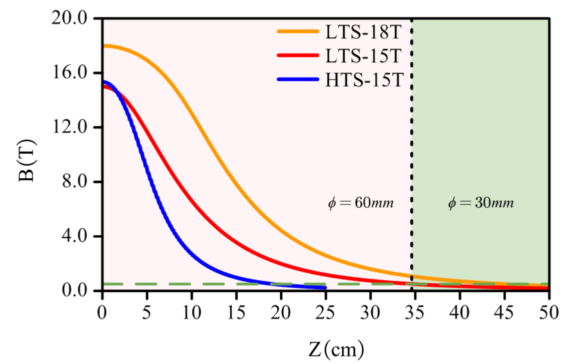

Figure 5: Magnetic field profiles of candidate SC AMD schemes.

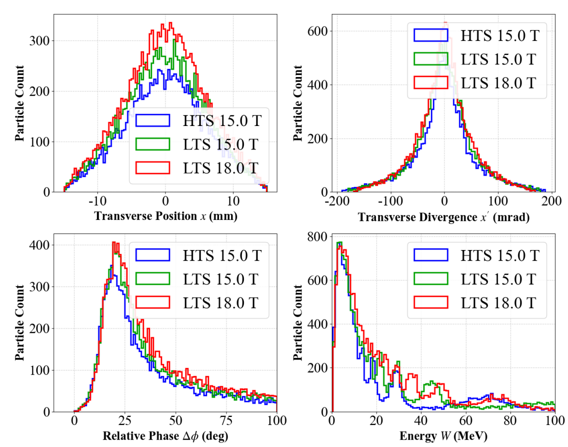

Figure 6: Phase-space distributions and yield comparison at the AMD exit for different schemes.

Phase-space analysis (Fig. 6) demonstrates that the resulting positron yield depends not only on the absolute intensity of the peak magnetic field, but also tightly on the specific longitudinal profile of the field. For configurations with the identical peak field of 15 T, the distinct decay rates between HTS and LTS directly differentiate their longitudinal phase tracking and collection efficiencies. Meanwhile, the 18 T LTS scheme achieves the highest transmission yield among the evaluated configurations, which is attributed to the synergistic combination of its superior peak field intensity and the enhanced global transverse confinement provided by its extended field profile for particles with large divergence angles.

CONCLUSION

In conclusion, this paper systematically investigated the dynamical influence of AMD longitudinal magnetic field distributions on positron yield for high-luminosity colliders. Parametric scans of conventional pulsed FCs demonstrate that the positron capture efficiency encounters a distinct saturation plateau once the peak field exceeds approximately 12 T to 13 T. Beyond this regime, simply increasing the pulsed field amplitude yields diminishing returns in transmission due to the inherent geometric and operational constraints of normal-conducting hardware.

To explore methods for overcoming this saturation limitation, candidate superconducting (SC) AMD architectures were evaluated. Among the investigated configurations, the 18 T LTS solenoid achieves the highest transmission yield. For configurations with an identical 15 T peak field, the 15 T LTS scheme exhibits a higher capture capability than the 15 T HTS scheme. This advantage is attributed to the extended longitudinal field profile of the LTS configuration, which provides a broader high-field region along the beam axis, thereby more effectively confining positrons with large transverse divergence angles.

It should be noted that this study is limited to the configuration where the conversion target is located precisely at the magnetic field peak. Optimizing the relative longitudinal position of the target with respect to the field profile represents an important design freedom. Due to space constraints in this manuscript, a detailed multi-parameter optimization of this spatial offset, integrated with downstream microwave accelerating structures, will be pursued in future full-process simulations to support the final technical selection of the high-luminosity SC AMD for the STCF.

REFERENCES

[1] A. V. Kulikov *et al.*, "SLC positron source pulsed flux concentrator", in *Proc. PAC'91*, San Francisco, CA, USA, May 1991, pp. 2005-2007. doi:10.1109/PAC.1991.164851

[2] L. Zang, M. Akemoto, S. Fukuda et al., Prototyping of the flux concentrator for SuperKEKB positron capture, in *Proc. 9th Annual Meeting of Particle Accelerator Society of Japan*, Osaka, Japan, 2012, pp. 1171–1173. IAEA-INIS Ref: 45037145.

[3] I. Chaikovska *et al.*, "Update on the FCC-ee Positron Source Design Studies", in *Proc. IPAC'23*, Venice, Italy, May 2023, pp. 201-204. doi:10.18429/JACoW-IPAC2023-MOPL095

[4] J. D. Liu *et al.*, "System design and measurements of flux concentrator and its solid-state modulator for CEPC positron source", *Nucl. Sci. Tech.*, vol. 32, no. 7, p. 77, 2021. doi:10.1007/s41365-021-00904-z

[5] Y. Enomoto *et al.*, "A new flux concentrator made of Cu alloy for the SuperKEKB positron source", in *Proc. IPAC'21*, Campinas, Brazil, May 2021, pp. 2954-2956. doi:10.18429/JACoW-IPAC2021-WEPAB134

[6] N. Vallis *et al.*, "Proof-of-principle e^+ source for future colliders," *Phys. Rev. Accel. Beams*, vol. 27, no. 1, p. 013401, 2024. doi:10.1103/PhysRevAccelBeams.27.013401

[7] S. Agostinelli *et al.*, "GEANT4—a simulation toolkit," *Nucl. Instrum. Methods Phys. Res., Sect. A*, vol. 506, no. 3, pp. 250–303, 2003. doi:10.1016/S0168-9002(03)01368-8

[8] K. Flöttmann, "ASTRA: A Space Charge Tracking Algorithm," Version 3, DESY, Hamburg, Germany, 2011. User manual available at https://www.desy.de/~mpyflo/

[9] Y. L. Han *et al.*, "Optimization of the CLIC positron source using a start-to-end simulation approach involving multiple simulation codes," *Nucl. Instrum. Methods Phys. Res., Sect. A*, vol. 928, pp. 83–88, 2019. doi:10.1016/j.nima.2019.03.044

[10] R. Chehab, "Experimental Studies of Positron Sources Using Multi-GeV Channelled Electrons at CERN and KEK," in *Advanced Radiation Sources and Applications*, H. Wiedemann, Ed. Dordrecht, Netherlands: Springer, 2006, pp. 357–371. doi:10.1007/1-4020-3450-4_30